Available online at www.sciencedirect.com

ScienceDirect

Progress in Natural Science: Materials International 24 (2014) 142–149

Progress in Natural Science Materials International

www.elsevier.com/locate/pnsmi
www.sciencedirect.com

Original Research

Structural, elemental, optical and magnetic study of Fe doped ZnO and impurity phase formation

S. Karamat[a,b,d,*], R.S. Rawat[a], P. Lee[a], T.L. Tan[a], R.V. Ramanujan[c]

[a]*Natural Science and Science Education, National Institute of Education, Nanyang Technological University, Singapore 637616, Singapore*
[b]*COMSATS Institute of Information Technology, Islamabad, Pakistan*
[c]*School of Material Science and Engineering, Nanyang Technological University, Nanyang Avenue, Singapore 639798, Singapore*
[d]*Department of Physics, Middle East Technical University, Ankara, Turkey*

Received in revised form 21 March 2013; accepted 2 August 2013
Available online 19 April 2014

Abstract

We have prepared a series of $(ZnO)_{1-x}(Fe_2O_3)_{x \leq 0.10}$ bulk samples with various concentrations of Fe dopant by ball milling and investigated their structural, compositional, optical and magnetic properties by means of X-ray diffraction (XRD), X-ray photoelectron spectroscopy (XPS), Raman spectrometer and vibrating sample magnetometer (VSM), respectively. Information about different impurity phases was obtained through Rietveld refinements of XRD data analysis. XPS results showed different valence states (Fe^{2+} and Fe^{3+}) supported by shaking satellite peaks in samples. With increasing Fe doping percentage, the crystal quality deteriorated and a shift of E_2 low band (characteristic of ZnO) has been observed in Raman spectra. Energy band gap estimated from reflectance UV–vis spectroscopy showed shift for all bulk samples. The magnetic behavior was examined using a vibrating sample magnetometer (VSM), indicating ferromagnetic behavior at room temperature (300 K). The effective magnetic moment per Fe atom decreases with increase in doping percentage which indicates that ferromagnetic behavior arises from the substitution of Fe ions in the ZnO lattice.

Keywords: Fe doped ZnO; Dilute magnetic semiconductor; Rietveld refinements; X-ray spectroscopy; Band gap; Magnetic moment

1. Introduction

Dilute magnetic semiconductors (DMSs) have gained a considerable attention from scientific community because of their wondering optical and magnetic properties which have applications in 'Spin electronics' also known as spintronics [1–4]. The utility of wide band gap DMSs in spintronics technology demands strongest interactions between ferromagnetic and semiconducting properties. The search for such a marvelous DMS which exhibits ferromagnetic and semiconducting properties at room temperature was initiated after theoretical estimations [1]. By using local spin density approximation (LSDA), it was suggested that ZnO has a potential to exhibit high Curie temperature when Mn would be doped in ZnO lattice. Dietl estimations gave understanding about the GaMnAs system but it shows inconsistency between theoretical estimations and the experimental results for the case of transition metal doped wide band gap semiconductor, such as ZnO [1]. After these predictions about the dilute magnetic semiconductors, simulations of Sato and Katayama-Yoshida [2] showed that FM could also be achieved in V, Cr, Fe, Co, and Ni doped ZnO.

Over last decade, most of the research efforts were devoted to Mn and Co doped ZnO systems [3,4]. Very few studies were reported for Fe doped ZnO; however, reports showed inconsistency in magnetic behavior of Fe doped ZnO. Some

*Corresponding author at: Natural Science and Science Education, National Institute of Education, Nanyang Technological University, Singapore 637616, Singapore.
E-mail address: shumailakaramat@gmail.com (S. Karamat).
Peer review under responsibility of Chinese Materials Research Society.

Production and hosting by Elsevier

http://dx.doi.org/10.1016/j.pnsc.2014.03.009
1002-0071/

reports showed ferromagnetic behavior at room temperature when prepared by mechanical alloying [5], co-precipitation [6] solid-state reaction and sol–gel method [7,8]. Recent work on Fe doped ZnO thin film showed ferromagnetic ordering above room temperature but this magnetic ordering develop due to short range Fe and Fe oxide regions in the host lattice instead of proper substitution in the lattice [9]. The diversity in magnetic behaviour of a Fe doped ZnO system could be primarily because of different sample preparation techniques. On the other hand, some reports show that Fe doped ZnO has an anti-ferromagnetic nature [10]. Han et al. showed the absence of ferromagnetism at room temperature in bulk Fe doped ZnO samples and observed room temperature ferromagnetism by additional Cu doping in the Fe doped ZnO system [11]. Shim et al. also found ferromagnetism in Fe doped ZnO with additional Cu doping with the claim that it is due to other secondary phases, i.e., $ZnFe_2O_4$ [12]. Therefore, a careful characterization of Fe doped ZnO is required to understand this complex and interesting system.

The main aim of the present work is to study the effect of different Fe doping percentages in ZnO for a bulk system. A detailed study of the bulk Fe doped ZnO system was carried out to investigate the change in the structural, compositional, vibrational, optical and magnetic properties of ZnO with varying doping percentages of Fe.

2. Experiments

In this study a series of bulk $(ZnO)_{1-x}(Fe_2O_3)_{x\le 0.10}$ samples were prepared by a ball milling technique. High purity powders of appropriate ratio were mixed and milled for 16 h at room temperature. After milling, powders were calcined for 14 h in air at 400 °C. The $(ZnO)_{1-x}(Fe_2O_3)_{x\le 0.10}$ calcined powders were ground, pelletized and sintered for 16 h at 900 °C in air ambience inside a furnace. X-ray diffraction of pellets was performed using a Shimazdu X-ray diffractometer with CuKα radiation. The lattice parameters and the percentage of secondary phases were obtained from Rietveld refinements [13,14]. The information about ZnO and impurity phases was also obtained from their vibrational modes in wave number range of 50–800 cm^{-1} using a Renishaw Raman Spectrophotometer. For excitation, a He–Ne laser (632 nm) was used with the incident laser power of 40 mW. Compositional analysis of Fe doped ZnO pellet samples was obtained by X-ray photoelectron spectroscopy (XPS) (Kratos Ultra) measurements. XPS spectra were recorded using monochromatized Al Kα radiation (1486.6 eV) and the binding energy (BE) values were calibrated with respect to C 1s peak of adventitious carbon (285.1 eV). Optical measurements were done by using a LAMBDA 950 UV/vis/NIR UV–visible spectrophotometer. Magnetic measurements were done at room temperature using a Lakeshore 7400 vibrating sample magnetometer.

3. Results and discussion

Fig. 1 shows XRD patterns for the bulk samples of $(ZnO)_{1-x}(Fe_2O_3)_{x\le 0.10}$ series. The dominant diffraction peaks indexed to wurtzite structure of ZnO with some additional peaks of a spinel $ZnFe_2O_4$ phase are marked with * as shown in Fig. 1.

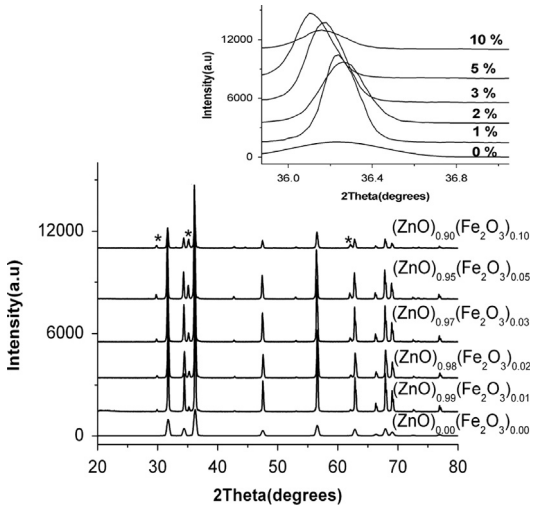

Fig. 1. XRD patterns for bulk samples of $(ZnO)_{1-x}(Fe_2O_3)_{x\le 0.10}$. The peaks labeled with * are that of spinel $ZnFe_2O_4$. Inset shows the random shift of (101) peak.

A random shift of (101) reflection peak of ZnO was observed for different doping concentrations of Fe. The shift of (101) reflection plane is an indication of different valence states of Fe ion substitution. In Fig. 1, the XRD patterns of $(ZnO)_{1-x}(Fe_2O_3)_x$ bulk samples show co-existence of ZnFeO (hexagonal) and $ZnFe_2O_4$ (spinel) phases, which may arise due to ball milling or heat treatment of samples. The quantitative information about the XRD patterns was obtained from Rietveld refinements. Rietveld refinement patterns for $(ZnO)_{1-x}(Fe_2O_3)_{x\le 0.10}$ series are shown in Fig. 2(a–e). For refinements, the patterns used were wurtzite hexagonal space group P63mc for ZnO along with franklinite (space group: Fd-3mZ) for $ZnFe_2O_4$. The cause of shift in (101) reflection peak is because of variation in lattice spacing a and c as shown in Table 1. The change in lattice spacing is because of different ionic radii of Fe ions substituted in the ZnO lattice. The XRD patterns also show an increase in $ZnFe_2O_4$ spinel phase percentage with increasing Fe doping which is due to the diffusion of Fe_2O_3 in the ZnO lattice. The percentage increase of spinel phase formation obtained from Rietveld refinements is shown in Table 2.

Therefore, from the results above, it is concluded that increasing doping percentage in ZnO not only causes the substitution of Fe ions in ZnO lattice but also promotes a competing process of spinel $ZnFe_2O_4$ formation which dominates with increasing doping percentage.

A detailed survey scan was done for all pellets which confirmed the presence of Zn and Fe 2p peaks along with O 1s. Survey scans are necessary for precise peak location and for accurate registration of line shapes. In order to get deeper insight about electronic structure of ZnO, after Fe incorporation, Zn 2p, Fe 2p and O 1s core peaks were measured for all samples in a systematic way. The present binding energies values for core peaks and the one mentioned in the literature for ZnO were found to be in good agreement [15]. The binding

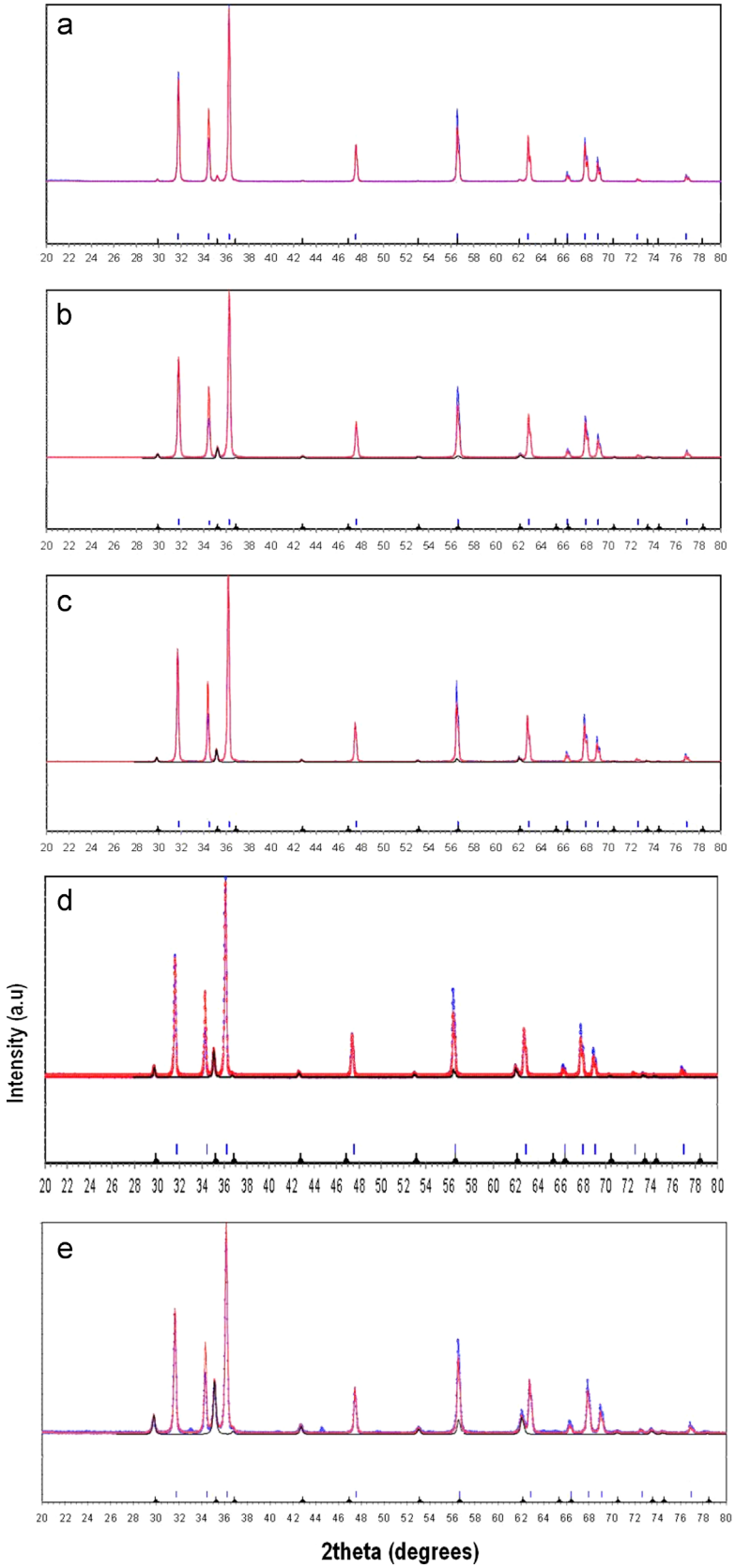

Fig. 2. (a–e) Rietveld refinements for $(ZnO)_{1-x}(Fe_2O_3)_x$ pellets for ($x \leq 10$).

Table 1
Lattice parameters for $(ZnO)_{1-x}(Fe_2O_3)_x$ pellets after refinements.

Material	a (Å)	c (Å)	Volume (Å^3)
$(ZnO)_{0.99}(Fe_2O_3)_{0.01}$	3.252	5.205	47.6776
$(ZnO)_{0.98}(Fe_2O_3)_{0.02}$	3.2503	5.2023	47.5971
$(ZnO)_{0.97}(Fe_2O_3)_{0.03}$	3.2505	5.2029	47.6103
$(ZnO)_{0.95}(Fe_2O_3)_{0.05}$	3.2507	5.2019	47.5867
$(ZnO)_{0.90}(Fe_2O_3)_{0.10}$	3.2487	5.2037	47.5647

Table 2
Impurity phase percentage obtained from Rietveld analysis for $(ZnO)_{1-x}(Fe_2O_3)_x$ pellets.

Materials	**Phases and their percentage**	
	Phase	Percentage
$(ZnO)_{0.99}(Fe_2O_3)_{0.01}$	ZnO	91.14
	$ZnFe_2O_4$	8.86
$(ZnO)_{0.98}(Fe_2O_3)_{0.02}$	ZnO	85.69
	$ZnFe_2O_4$	14.31
$(ZnO)_{0.97}(Fe_2O_3)_{0.03}$	ZnO	82.42
	$ZnFe_2O_4$	17.58
$(ZnO)_{0.95}(Fe_2O_3)_{0.05}$	ZnO	70.70
	$ZnFe_2O_4$	29.30
$(ZnO)_{0.90}(Fe_2O_3)_{0.10}$	ZnO	52.32
	$ZnFe_2O_4$	47.68

energies of Zn $2p_{3/2}$, as shown in Fig. 3, are located at 1021.3, 1021.2, 1021.0, 1022.2 and 1021.0 eV for 1%, 2%, 3%, 5% and 10% Fe doped ZnO, respectively. The binding energy of central Zn $2p_{3/2}$ shows asymmetrical behavior for Fe doped ZnO samples. This asymmetrical change of binding energy is related to Zn–O bond length change, which may be due to the incorporation/substitution of bigger sized Fe ion (0.63 Å) into ZnO lattice. We de-convolute all Zn $2p_{3/2}$ core peaks for bulk samples in order to resolve the inconsistency in binding energy values, shown in Fig. 3(a–e). In Fig. 3(a), the central Zn $2p_{3/2}$ core peak of $(ZnO)_{0.99}(Fe_2O_3)_{0.01}$ at binding energy of 1021.27 eV is de-convoluted into three peaks by Gaussian peak fitting having binding energy of 1020.5, 1021.2 and 1021.9 eV. The de-convoluted peaks at 1020.5 and 1021.2 eV can be considered due to Zn in ZnO. The binding energy peak of 1021 eV is dominant in the whole spectrum. It may be due to the variation of Zn–O broken bonds when Zn ions were substituted by Fe ions. It is explained in more detail as follows. Ideally, zinc cations are arranged in tetrahedral co-ordination with four oxygen ions in the case of bulk samples, assumed as zero bond breakage. When ions of different elements substitute Zn ions, the bonds start breaking up. With increase in broken bonds, the quantity of charge transfer from zinc to oxygen ions reduces, which causes a decrease in the binding energy values of core electron of Zn ions. Considering this fact, the binding energy peak at 1021.2 eV may be due to broken bonds of Zn ions. The peak appeared at 1020.5 eV can be assigned due to two broken bonds [16]. The de-convoluted peak at higher energy side, i.e., at 1021.9 eV has an ambiguous impact. This peak could be due to Zn in ZnO lattice or in $ZnFe_2O_4$. According to the literature [15], all peaks show the Zn presence in ZnO, and the expected Zn $2p_{3/2}$ core peak of $ZnFe_2O_4$ exists at 1021.4 eV, which shifts in our case. The binding energy also varies with the size of the ions that substitute Zn. When Fe^{2+} ion of bigger ionic radius (0.63 Å) substitutes Zn^{2+} (0.60 Å) ion in lattice, the bond length reduces, which increases the binding energy between the atoms. So, the peak at 1021.9 eV is most probably due to the overlapping of Zn peak in ZnO and $ZnFe_2O_4$. From XPS results, the relative Zn percentage in a ZnO phase is 72.8% and in a mixed phase (ZnO and $ZnFe_2O_4$) Zn percentage is 27.2%. In Fig. 3(b), the central Zn $2p_{3/2}$ core peak of $(ZnO)_{0.98}(Fe_2O_3)_{0.02}$ at binding energy of 1021.1 eV is de-convoluted into three peaks by Gaussian peak fitting having binding energies of 1020.6, 1021.1 and 1021.7 eV. The de-convoluted peaks at 1020.6 and 1021.1 eV can be considered due to Zn in ZnO and at 1021.4 eV; again there is combination of Zn peak in ZnO and $ZnFe_2O_4$. The relative Zn percentage in the ZnO phase is 78.4% and in overlapped region Zn percentage is 21.6%. Similar behavior of Zn peak was observed for $(ZnO)_{0.97}(Fe_2O_3)_{0.03}$, $(ZnO)_{0.95}(Fe_2O_3)_{0.05}$ and $(ZnO)_{0.90}(Fe_2O_3)_{0.10}$ compositions.

Fig. 4(a–e) shows the XPS spectrum of Fe 2p core peaks of $(ZnO)_{1-x}(Fe_2O_3)_x$ samples having different Fe percentages. Fe $2p_{3/2}$ and $2p_{1/2}$ doublet at 710.5 and 724.4, 710.93 and 724.0, 710.4 and 724.2, 710.7 and 724.7, and 710.3 and 723.8 eV along with their shake-up resonance transitions (satellite) are observed for 1%, 2%, 3%, 5% and 10% Fe doped ZnO samples, respectively. Binding energy shows the difference of 13.5 eV between Fe $2p_{3/2}$ and $2p_{1/2}$ peaks which resulted from spin–orbit coupling. From previous data, the difference in binding energy values of peaks would be around 13.10 eV for Fe–Fe clusters [17]. It gives us enough evidence to state confidently that Fe clustering is not present in our samples.

The oxidation states of Fe^{2+} and Fe^{3+} ions can be distinguished from the binding energy values of Fe 2p. The de-convolution of Fe $2p_{3/2}$ reveals two peaks at 710.8 and 711.5, 710.6 and 713.0, 710.58 and 712.84, 711.0 and 713.7 and 710.6 and 713.2 eV for 1%, 2%, 3%, 5% and 10% doped samples. The difference in binding energy of Fe^{2+} and Fe^{3+} is quite small and it is important to resolve the broad iron core-level spectra in oxide matrices by de-convolution of peaks. The peaks on higher energy side after de-convolution show the presence of Fe^{3+} valence state and peaks toward lower side indicate Fe^{2+} valence state in the samples. The Fe $2p_{3/2}$ core peak position shows shift toward higher binding energies with reference to elemental Fe 706.7 eV [18]. The appearance of Fe $2p_{3/2}$ core peaks points towards the presence of Fe–O bonding in samples. The presence of satellite peaks at relatively higher binding energies of 717.3 and 728.6, 718.0 and 728.6, 718.0 and 731.92, 718.0 and 732.1 and 718.1 and 731.7 eV also confirms the divalent and trivalent states of Fe ions in all investigated samples.

XPS core peak spectrum of O 1s for $(ZnO)_{0.99}(Fe_2O_3)_{0.01}$ pellets is shown in Fig. 5. Similar to Zn $2p_{3/2}$, the O 1s peak

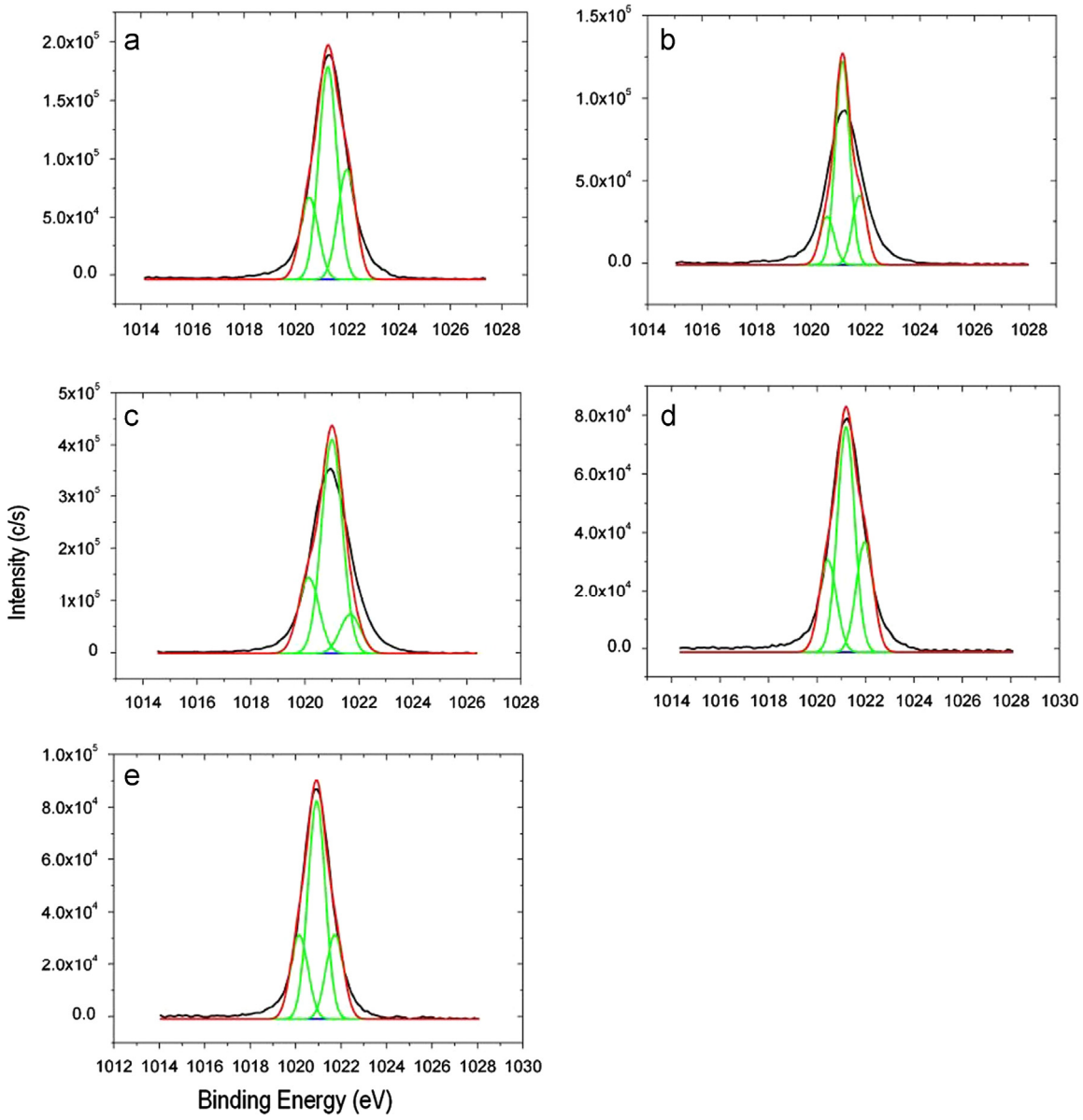

Fig. 3. XPS spectrum around the Zn $2p_{3/2}$ core level of (a) $(ZnO)_{0.99}(Fe_2O_3)_{0.01}$, (b) $(ZnO)_{0.98}(Fe_2O_3)_{0.02}$, (c) $(ZnO)_{0.97}(Fe_2O_3)_{0.03}$, (d) $(ZnO)_{0.95}(Fe_2O_3)_{0.05}$ and (e) $(ZnO)_{0.90}(Fe_2O_3)_{0.10}$ pellets.

shows asymmetrical trend, which indicates the presence of multi-component oxygen species mostly appearing at the near-surface region. The typical O 1s peak can be fitted by three Gaussians peaks for all samples. The centered peaks around 532.0 eV may appear because of chemisorbed oxygen. The peak around 529.4 eV is due to Zn–O bonds and the peak around 530.5 eV is due to the ZnFeO crystal lattice oxygen.

The de-convolution of XPS core peaks of Zn, Fe and O shows that our samples contain different valence states of the elements. The change in binding energy values of Zn core peaks shows different Fe valence ions substitution in ZnO lattice. The change in Fe binding energy values further indicates different Fe valence ions. Moreover, oxygen core peaks show the change in binding energy from standard value due to breaking of Zn–O bonding assuring that the Fe ions have successfully substituted/intermixed/diffused with Zn ions in the ZnO lattice.

Raman spectroscopy is used to find out the effect of dopant in ZnO structure. ZnO, a wide bandgap semiconductor, has a wurtzite crystal structure which belongs to C_{6v}^4 space group. The Raman-active zone-center optical phonons are $A_1+2B_1+E_1+2E_2$ predicted from the group theory. The polar phonons of A_1 and E_1 symmetries show different wave numbers for transverse-optical (TO) and longitudinal-optical (LO) phonons. Non-polar phonon modes show two wave numbers having E_2 symmetry: E_2 (high) which is characteristic of oxygen atoms and E_2 (low) which is characteristic of Zn sublattice. B_1 modes belong to IR and Raman inactive (silent modes). These phonon modes have been reported in the Raman scattering spectra of bulk ZnO [19,20].

In Raman spectra of $(ZnO)_{1-x}(Fe_2O_3)_{x\leq 0.05}$ bulk samples, the 332 cm^{-1} peak is due to an A_1(TO) mode which shows second-order Raman processes (multiple-phonon processes).

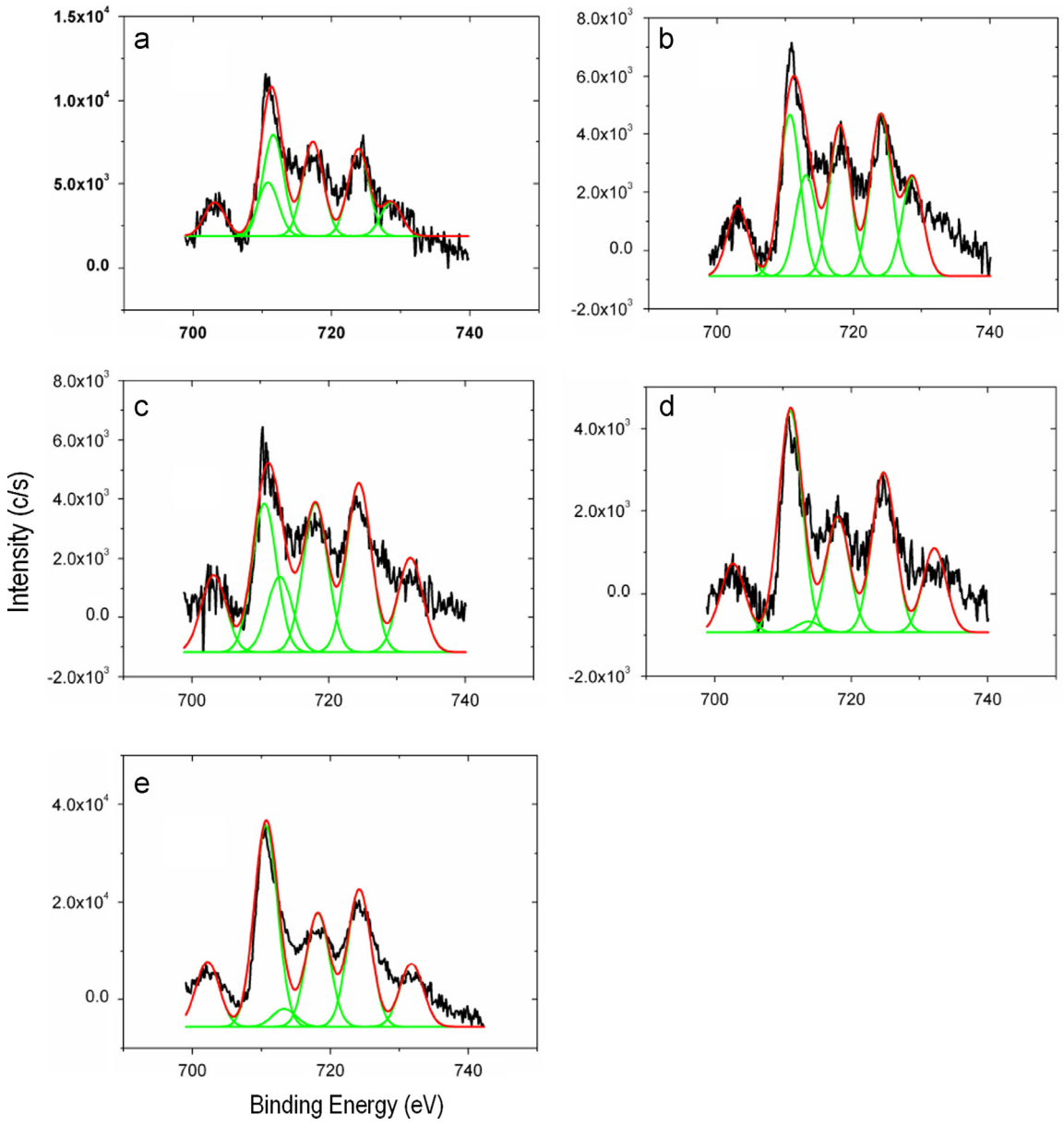

Fig. 4. XPS spectrum around Fe 2p core peak for (a) $(ZnO)_{0.99}(Fe_2O_3)_{0.01}$, (b) $(ZnO)_{0.98}(Fe_2O_3)_{0.02}$, (c) $(ZnO)_{0.97}(Fe_2O_3)_{0.03}$, (d) $(ZnO)_{0.95}(Fe_2O_3)_{0.05}$ and (e) $(ZnO)_{0.90}(Fe_2O_3)_{0.10}$ pellets.

The 377.1 cm^{-1} peak is due to an E_1 (TO) mode and a phonon mode occurring at 437 cm^{-1} corresponds to an E_2 (high) mode of ZnO. The E_2 (low) mode also shows a small peak at 98 cm^{-1} which is magnified for clear visibility in the inset of Fig. 6. With increase in Fe doping percentage, the intensity of the E_2 (low) mode decreases. E_2 (low) is due to first order Raman processes; change in Fe doping affects phonon vibrations. Moreover, the undoped ZnO sample, not shown here, exhibits E_2 (low) peak at 99.2 cm^{-1}, while the peaks with doping showed random shift in peak position with respect to undoped ZnO sample which is due to different phase formations and Zn–O bond breakage. These observations confirm that Fe incorporation induces disorder in the ZnO crystal lattice [21]. Moreover, this figure also shows that the additional broad band at 646 cm^{-1} corresponding to Fe doped ZnO mostly appears at high temperature [22]. The broadening in the peak might indicate the overlapping of an Fe_3O_4 (magnetite) mode appearing at 668 cm^{-1} and the Fe doped ZnO mode appearing at 641 cm^{-1} [23]. But from other investigations (XPS and XRD), we did not get any information about magnetite, so most probably this phase is due to the overlapping of Fe doped ZnO and spinel phase. The other observable fact is the shifting of mode positions from the most reported positions of ZnO modes (E_2 (low)), which suggests that Fe ions are substituted in the ZnO lattice. The tetrahedral sites in the wurtzite structure are occupied by Zn ions which generate new crystalline lattice defects when substituted by ions of magnetic dopants. The lattice defects induce structural disorder which breaks the

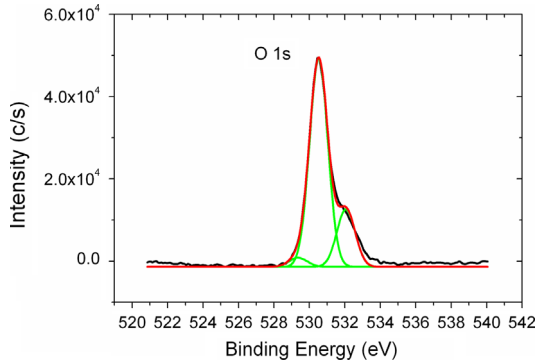

Fig. 5. XPS spectrum around O 1s core peak for $(ZnO)_{0.99}(Fe_2O_3)_{0.01}$ pellets.

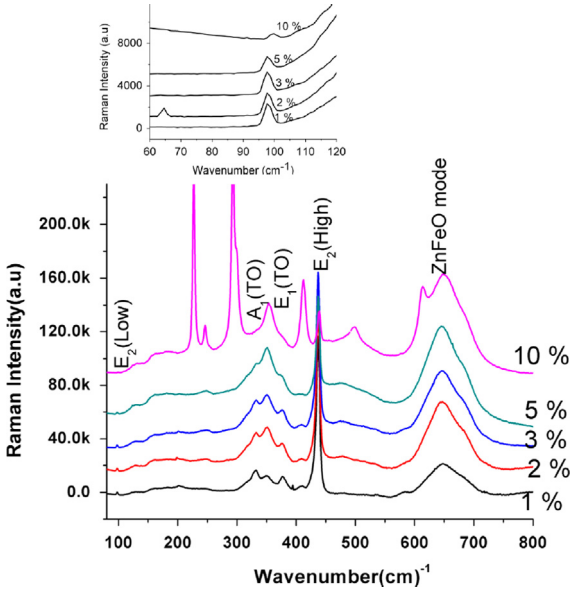

Fig. 6. Raman spectra for $(ZnO)_{1-x}(Fe_2O_3)_{x\le 0.05}$ series of bulk samples measured at room temperature.

translational symmetry of the allowed phonons of the host lattice, which results in a variation in the Raman line shape [24].

We have estimated the optical band gap of the $(ZnO)_{1-x}(Fe_2O_3)_{x\le 0.10}$ pellets from the reflectance spectra obtained by the UV–visible spectrophotometer. For optical band gap measurements, the diffuse reflectance, R, of the pellets can be obtained by using the Kubelka–Munk function $F(R)$, where $F(R)=(1-R)^2/2R$ [25]. To measure the band gap we plotted data $(F(R))^{1/n}$ and photon energy $h\nu$, with $n=1/2$ because of ZnO direct allowed band gap transitions (Fig. 7). Another notable point is that the indirect transitions appear around 2 eV which indicate the presence of the spinel phase. The values of band gap in the form of energies were estimated by taking the intersection of the extrapolated lines from the linear vertical and horizontal regions near the band edge. The estimated band gap values are 3.18, 3.024, 3.044, 3.03, 3.08 and 3.22 eV for 0%, 1%, 2%, 3%, 5% and 10% Fe doped ZnO samples, respectively. These estimated values for all samples show red-shift with respect to bulk ZnO sample, except for 10% Fe doped ZnO sample which exhibits that blue-shift as band gap of our bulk ZnO is about 3.18 eV. It is reported that the cause of red-shift in the band gap values may be due to strong sp–d exchange interactions. These exchange interactions arise between band electrons of ZnO and the localized d electron of Fe atoms when Fe ions substituted some of the Zn ions in ZnO.

Magnetic characterizations for the bulk samples were done by using VSM at room temperature. Fig. 8 shows the hysteresis graph for $(ZnO)_{1-x}(Fe_2O_3)_{x\le 0.10}$ pellets, where the inset shows the magnified spectra revealing the soft ferromagnetic nature. It has been observed that our samples did not show full saturation; this effect appears due to the ambiguous nature of a ZnFeO phase which contributes in both ferromagnetic and paramagnetic behaviors. It has also been shown in previous studies that the $ZnFe_2O_4$ phase exhibits

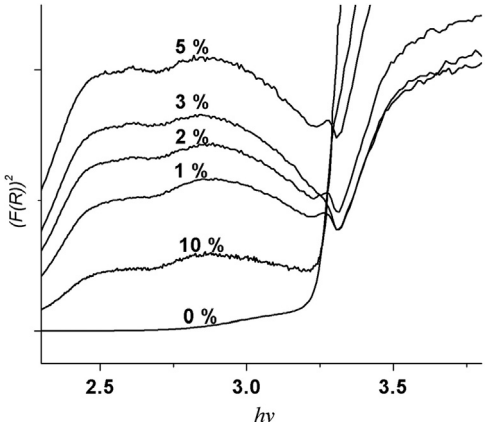

Fig. 7. Plot of $(F(R))^2$ and photon energy for band gap calculation of $(ZnO)_{1-x}(Fe_2O_3)_{x\le 0.10}$ bulk samples.

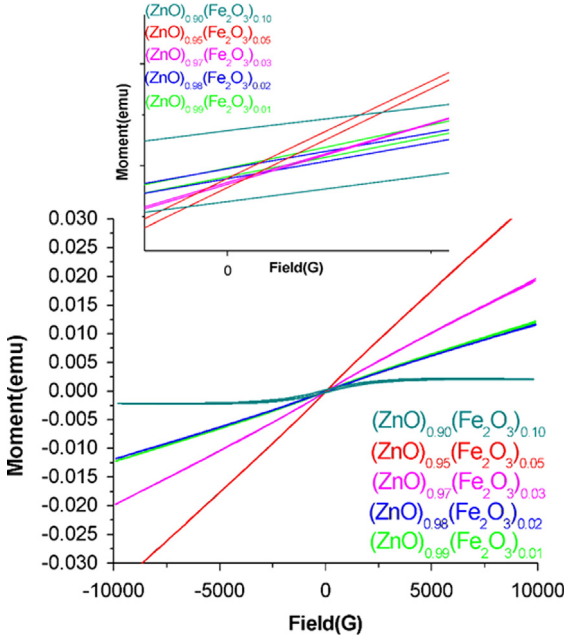

Fig. 8. M–H curves for $(ZnO)_{1-x}(Fe_2O_3)_{x\le 0.10}$ bulk samples. Inset shows magnified spectra which reveals ferromagnetic behavior.

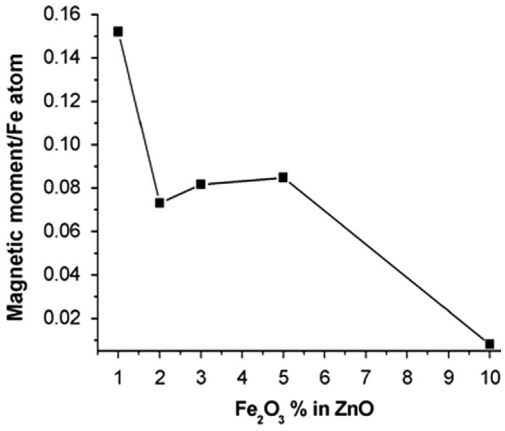

Fig. 9. Magnetic moment in $(ZnO)_{1-x}(Fe_2O_3)_{x \leq 0.10}$ bulk samples.

anti-ferromagnetic behavior which may suppress the ferromagnetic signal [6]. Fig. 9 shows the trend of saturated magnetic moment versus Fe doping percentage. With increase in Fe doping (from 1% to 10%), a considerable decrease in the magnetic moment per Fe atom has been noticed. The XRD results suggest that the substitution of Fe ions in the ZnO lattice forms a solid solution instead of precipitates. The existence of a secondary phase observed in XRD, that is, $ZnFe_2O_4$ exhibits antiferromagnetic nature [12]. However, the increase/decrease in the lattice parameter with increasing doping percentage indicates that it is not only due to Fe^{2+} ions but also due to Fe^{3+} ions substitution in the ZnO lattice. In view of the Fe^{3+} ions substitution for Zn^{2+}, some carrier-related mechanisms, such as RKKY–Zener interaction, double-exchange–Zener interaction and bound magnetic polarons (BMP) theory, may explain well the cause of magnetism. It might be possible that the substitution of Fe^{3+} contributes in paramagnetic signal. Further research on this system is required in the future to clear more of the unresolved issues.

4. Conclusions

In this study, structural, compositional, vibrational, optical and magnetic properties of $(ZnO)_{1-x}(Fe_2O_3)_{x \leq 0.10}$ series of pellets were studied. Quantitative analysis of the XRD data obtained for samples showed an increase in the impurity phases with increasing percentage of Fe. The variation in lattice parameters showed the effective substitution of Zn ions by different valence states of Fe ions. The XPS results showed a change in Zn binding energy values which is due to the alteration in zinc bonding. The binding energy analysis of Fe core peaks confirmed the presence of different valence states. The band gap shift was observed in all Fe doped pellets. Raman spectroscopy gave information about the vibrational modes which showed the influence of dopants on ZnO lattice and the information related to secondary phases. The additional mode appearing in the spectra of Fe doped ZnO at 646 cm^{-1} hints towards the presence of magnetic ions. *M–H* curves exhibit ferromagnetism with slight paramagnetic contribution. Increasing Fe content from 1 to 10 at% resulted in a decrease in the magnetic moment per Fe atom, which predicted that ferromagnetism arises due to substitution of Fe ions in the lattice.

Acknowledgments

The authors are grateful to the National Institute of Education/Nanyang Technological University, Singapore, for providing AcRF Grant RI 17/03/RSR. One of us, S Karamat, would like to thank NIE/NTU for providing the research scholarship.

References

[1] T. Dietl, H. Ohno, F. Matsukura, J. Cibert, D. Ferrand, Science 287 (2000) 1019.
[2] K. Sato, H. Katayama-Yoshida, Jpn. J. Appl. Phys. 39 (2) (2000) L555.
[3] S.W. Jung, S.J. An, G.C. Yi, Appl. Phys. Lett. 80 (2002) 4561.
[4] P. Sharma, K. Sreenivas, K.V. Rao, J. Appl. Phys. 93 (2003) 3963.
[5] Y. Lin, D. Jiang, F. Lin, W. Shi, X. Ma, J. Alloys Compd. 436 (2007) 30.
[6] Y.Q. Wang, S.L. Yuan, L. Liu, P. Li, X.X. Lan, Z.M. Tian, J.H. He, S.Y. Yin, J. Magn. Magn. Mater. 320 (2008) 1423.
[7] G.Y. Ahn, S.I. Park, S.J. Kim, B.W. Lee, C.S. Kim, IEEE Trans. Magn. 41 (2005) 2730.
[8] G.Y. Ahn, S.I. Park, C.S. Kim, J. Magn. Magn. Mater. 303 (2006) e329.
[9] S.D. Yoon, Y. Chen, J. Appl. Phys. 99 (8) (2006) M109.
[10] S.W. Yoon, S.B. Cho, S.C. We, S. Yoon, B.J. Suh, H.K. Song, J. Shin, J. Appl. Phys. Lett. 81 (2002) 4212.
[11] S.J. Han, J.W. Song, C.-H. Yang, S.H. Park, J.-H. Park, Y.H. Jeong, Appl. Phys. Lett. 81 (2002) 4212.
[12] J.H. Shim, T. Hwang, S. Lee, Appl. Phys. Lett. 86 (2005) 082503.
[13] J. Blasco, F. Bartolome, L.M. Garcia, J. Garcia, J. Mater. Chem. 16 (2006) 2282.
[14] J. Rodrı´guez-Carvajal, Physica B 192 (1992) 55.
[15] ⟨http://srdata.nist.gov/xps/⟩.
[16] Y.Y. Tay, S. Li, C.Q. Sun, P. Chen, Appl. Phys. Lett. 88 (2006) 173118.
[17] S.Y. Seo, C.H. Kwak, Y.B. Lee, S.H. Kim, S.H. Park, S.W. Han, J. Korean Phys. Soc. 52 (2008) 1.
[18] Q.J. Feng, D.Z. Shen, J.Y. Zhang, Y.M. Lu, Y.C. Liu, X.W. Fan, Mater. Chem. Phys. 96 (2006) 158.
[19] N. Ashkenov, B.N. Mbenkum, C. Bundesmann, V. Riede, M. Lorenz, D. Spemann, E.M. Kaidashev, A. Kasic, M. Schubert, M. Grundmann, J. Appl. Phys. 93 (2003) 126.
[20] J.F. Scott, Phys. Rev. B 2 (1970) 1209.
[21] C. Wang, Z. Chen, Y. He, L. Li, D. Zhang, Appl. Surf. Sci. 255 (2009) 6881.
[22] R.Y. Sato-Berru, A. Vazquez-Olmos, A.L. Fernandez-Osorio, S. Sotres-Martınez, J. Raman Spectrosc. 38 (2007) 1073.
[23] C. Bundesmann, N. Ashkenov, M. Schubert, D. Spemann, T. Butz, E.M. Kaidashev, M. Lorenz, M. Grundmann, Appl. Phys. Lett. 83 (2003) 1974.
[24] K. Samanta, P. Bhattacharya, R.S. Katiyar, Phys. Rev. B 73 (2006) 245213.
[25] J. Hays, K.M. Reddy, N.Y. Graces, M.H. Engelhard, V. Shutthanandan, M. Luo, C. Xu, N.C. Giles, C. Wang, S. Thevuthasan, A. Punnoose, J. Phys.: Condens. Matter 19 (2007) 266203.